Eastward-moving Equatorial Modons in moist-convective Shallow-Water Models

Masoud Rostami, Vladimir Zeitlin

Eastward-moving Equatorial Modons in moist-convective Shallow-Water Models

MASOUD ROSTAMI[a,b], VLADIMIR ZEITLIN[a]

[a]Laboratoire de Météorologie Dynamique (LMD)/IPSL, Sorbonne Université and Ecole Normale Supérieure (ENS), Paris, France
[b] Institute for Geophysics and Meteorology (IGM), University of Cologne, Cologne, Germany

This is the Author's Original Manuscript (AOM); that is, the manuscript in its original form; a "preprint" . The Version of Record of this manuscript has been accepted for publication by the Journal of *Geophysical & Astrophysical Fluid Dynamics*, published by *Taylor & Francis*. The publisher's version is available at https://doi.org/10.1080/03091929.2020.1805448.

Geophysical and Astrophysical Fluid Dynamics
Vol. 00, No. 00, 00 Month 20xx, 2–22

Eastward-moving Equatorial Modons in moist-convective Shallow-Water Models.

MASOUD ROSTAMI† ‡ and VLADIMIR ZEITLIN †
† Laboratoire de Météorologie Dynamique/Sorbonne Université/ Ecole Normale Supérieure (ENS)/CNRS, 24 Rue Lhomond, 75005 Paris, France
‡ Institute for Geophysics and Meteorology, University of Cologne, 50969 Cologne, Germany

(*Received 00 Month 20xx; final version received 00 Month 20xx*)

It is shown that steady large-scale slowly eastward-moving twin-cyclone coherent structures, the equatorial modons, exist in both one- and two layer versions of the rotating shallow water model on the equatorial beta plane. They arise via the process of "ageostrophic adjustment" from the analytic asymptotic modon solutions of the vorticity equation obtained in the limit of small pressure perturbations. Evolution of these structures in adiabatic and moist-convective environments, and also in the presence of topography is analyzed, showing their robustness in the one-layer model. It is demonstrated that moist convection enhances and helps maintain the modons. In the two-layer model the barotropic and quasi-barotropic modons display similar to one-layer modon features, while increasing baroclinicity leads to eventual loss of coherence and arrest of the eastward propagation. Some features of equatorial modons resemble those observed in the Madden-Julian Oscillation events in tropical atmosphere, which hints at their possible relevance to the dynamics of this phenomenon.

Keywords: Equatorial Waves, Madden Julian Oscillation, Modon, Moist Convection, Rotating Shallow Water Model

1. Introduction

Atmospheric dynamics in the equatorial regions of rotating planets significantly differs from that in higher latitudes due to the simple fact that the rotation axis lies in the tangent plane to the equator. As is well known starting from the pioneering paper by Matsuno (1966), equatorial dynamics is dominated by specific equatorial waves, e.g. (Gill 1982). These waves are well identified in meteorological *in situ* and satellite observations, e.g. (Wheeler and Kiladis 1999). Yet, both kinds of observations reveal slow eastward-propagating structures which do not fall in any class of equatorial waves. They were identified as periodically arising large-scale patterns of enhanced deep convection which are slowly moving from the Indian Ocean over the maritime continent and dying out in the Pacific, the Madden-Julian Oscillation (MJO). After its discovery (Madden and Julian 1972), much was learnt about its structure and properties, e.g. Zhang (2005). Yet dynamical nature of MJO is not fully understood (Zhang 2005) and, in particular, there is no clear answer to the question why MJO events are slowly moving eastward. Climate models have difficulties in reproducing them, e.g. (Kim et al. 2011). The Kelvin waves, the only species of the equatorial waves that can produce steady large-scale

Corresponding author. Email: zeitlin@lmd.ens.fr Address: LMD-ENS, 24 Rue Lhomond, 75005 Paris, France

eastward-moving structures, have much faster velocity than MJO (Straub and Kiladis 2002). There exist simplified models of MJO, either quasi-linear, e.g. Majda and Stechman (2009), Sobel and Maloney (2012), or nonlinear Haertel et al. (2013), all of them heavily relying on the dynamical role of moist convection.

The question however arises, whether there exist "dry" dynamical structures moving slowly eastwards along the equator, which could provide a dynamical "backbone" of the MJO events. The spectrum of linear equatorial waves being well established, such objects should be necessarily nonlinear. There do exist steady eastward-moving structures in a fluid layer in the mid-latitude tangent- plane approximation, the so-called modons, exact dipolar solutions of the quasi-geostrophic (QG) equations discovered by Larichev and Reznik (1976). Although the classical modons were found analytically in the QG approximation, it was shown first by a computer-assisted analysis (Kizner et al. 2008) and then by direct numerical simulations (Ribstein et al. 2010) that corresponding solutions exist also in the parent rotating shallow water (RSW) model on the f- plane. The QG modon solutions were extended to the full sphere (Verkley 1984, Tribbia 1984) in the framework of equivalent barotropic model, which is structurally close to QG. In their pioneering paper, Yano and Tribbia (2017) came up with an idea that the MJO could be related to such a modon in spherical geometry and showed that, like on the tangent plane (Ribstein et al. 2010), the equivalent barotropic modon persists in the parent RSW model on the sphere. Yet, the archetype model for understanding dynamics of the tropical atmosphere is RSW on the equatorial beta-plane, e.g. Matsuno (1966). For example, the spectrum of convectively coupled equatorial waves, including MJO, is studied by projection onto the wave-spectrum of the RSW model (Wheeler and Kiladis 1999, Straub and Kiladis 2002). The idea, thus, arises to look for modons in this model. However, it encounters an obstacle from the very beginning because a consistent QG approximation at the equator is problematic, e.g. James (1994), so the known QG modon solutions can not be directly borrowed. We should emphasize at this point, that coherent *westward-propagating* dipoles were found in the RSW model on the equatorial beta-plane by Boyd (1985), and were also called modons. However, their nature is different, as they correspond to the KdV solitons of weakly nonlinear long equatorial Rossby waves, see (LeSommer et al. 2004). A conjecture that eastward propagating modons could exist was also formulated by Boyd (1985). We will discuss this point in Sect. 3 below.

Let us also emphasize that the applications of the RSW model on the equatorial beta-plane are not limited to tropical meteorology. The related equatorial wave dynamics is regularly invoked for explanations of the observations in the equatorial regions of planetary atmospheres, e.g. (Showman and Dowling 2000, Legarreta et al. 2016, Sanchez-Lavega et al. 2017).

Our main observation (Rostami and Zeitlin 2019a) is that there exist a dynamical regime in the RSW model, corresponding to the so-called long-wave approximation in oceanography (Gill 1982), which arises in the limit of small pressure variations and gives, to the leading order, a vorticity equation which does allow for modon solutions. This quasi-barotropic regime is the RSW analog of Charney (1963) non-divergent balance model for equatorial atmosphere. The relevance of this model to large-scale tropical motions is supported by scale and data analyses (Yano and Bonazzola 2009, Yano et al. 2009). Modon solutions in this regime were constructed in Rostami and Zeitlin (2019a). Following the strategy of Ribstein et al. (2010), these asymptotic solutions were then used to initialize high-resolution numerical simulations with the full RSW model, and to show that coherent dipolar steady eastward-moving structures, the RSW modons, do arise and persist. However, the domain of attraction of such modon solutions seems to be limited as they do not arise without added dipolar vorticity component from initial localized circular pressure anomalies, even if these latter have considerable amplitudes. The modon configurations, however do arise from such configurations in the presence of moist-convective feedback (Rostami and Zeitlin 2019b).

Below we recall the derivation of equatorial modon solutions in one-layer RSW and present numerical simulations illustrating the influence of the effects of moisture and topography on their behavior. We show that topographic obstacles of reasonable amplitude do not disrupt the modons, and that inclusion of moisture, with condensation and evaporation, enhances the modons, and produces some specific convective and condensation patterns. We then turn to baroclinic generalizations of one-layer modons, and look for similar solutions in the two-layer equatorial RSW model. We analyze different parameter regimes in this model, under the same hypothesis of small pressure variations, and explore the possibilities of having coherent dipolar solutions. We show that such asymptotic solutions do exist, verifying layer-wise in the leading order the same vorticity equation as in the one-layer RSW. We then follow the same strategy as in the one-layer case, and initialize high-resolution numerical simulations with well-balanced finite-volume scheme for two-layer RSW equations on the equatorial beta-plane with the velocity fields corresponding to such asymptotic solutions. The simulations reveal that only close to barotropic initializations, i.e. those with the same in each layer, or close to, initial asymptotic modons, give rise to slowly eastward-moving two-layer RSW modons, while baroclinic, i.e. with asymptotic modons of essentially different size and/or intensity, initializations result in dipolar structures which are eventually turning westward and becoming equatorial Rossby-wave packets.

The paper is organized as follows. We first recall the theory of barotropic equatorial modons in one-layer equatorial RSW, and then analyze its generalization to the two-layer case in Sect. 2. We present the results of numerical simulations initialized with asymptotic modon solutions in both one- and two-layer cases, and in both "dry" and moist-convective environments in Sect. 3. Section 4 contains summary and discussion.

2. Modons in one- and two-layer RSW models: theory

2.1. *One-layer configuration*

2.1.1. *From one-layer RSW to barotropic model*

In this Section we recall the construction of equatorial modons which was sketched in Rostami and Zeitlin (2019a). The RSW model we are using should be understood as vertically averaged primitive equations in pseudo-height pressure coordinates (Zeitlin 2018), and can be extended to include water vapor with condensation and related latent heat release (Bouchut et al. 2009), as well as surface evaporation (Lahaye and Zeitlin 2016, Rostami and Zeitlin 2017). Liquid water, precipitation, vaporisation and related cooling can be also incorporated into the model, as well as vertical structure, see Rostami and Zeitlin (2018) for these generalizations, and references therein for previous successful applications of the model. Below we recall the approximations leading to the Charney regime in one-layer RSW model on the equatorial beta-plane following Rostami and Zeitlin (2019a).

The "dry" one-layer RSW equations in the equatorial beta- plane with no dissipation read:

$$\partial_t \mathbf{v} + \mathbf{v} \cdot \nabla \mathbf{v} + \beta y \, \hat{\mathbf{z}} \wedge \mathbf{v} + g \nabla h = 0 \,, \tag{1}$$

$$\partial_t h + \nabla \cdot [\mathbf{v}(h - b)] = 0 \,, \tag{2}$$

where $\nabla = (\partial_x, \partial_y)$, $\mathbf{v} = (u, v)$, u is zonal and v- meridional components of velocity, h is thickness in pseudo-height coordinates, $b > 0$ represents topography, β is the meridional gradient of the Coriolis parameter, and $\hat{\mathbf{z}}$ is a unit vertical vector. We introduce a nonlinearity parameter λ, which measures the amplitude of pressure variations $h = H(1 + \lambda\eta)$, where H is the unperturbed thickness, and rewrite the momentum equations correspondingly:

$$\partial_t \mathbf{v} + \mathbf{v} \cdot \nabla \mathbf{v} + \beta y \, \hat{\mathbf{z}} \wedge \mathbf{v} + gH\lambda \nabla \eta = 0 \,, \tag{3}$$

where we omitted topography, which would be reintroduced later. We then choose the same spatial and velocity scales in both zonal and meridional directions $(x, y) \sim L$, $(u, v) \sim V$, and choose the time-scale as: $t \sim (L/V)$. Notice that such uniform in zonal and meridional directions scaling differs from the traditionally used one, cf. Gill (1980), LeSommer et al. (2004). The non-dimensional momentum equations are:

$$\partial_t \mathbf{v} + \mathbf{v} \cdot \nabla \mathbf{v} + \overline{\beta} y \, \hat{\mathbf{z}} \wedge \mathbf{v} + \frac{gH\lambda}{V^2} \nabla \eta = 0 \,, \tag{4}$$

where we introduced a non-dimensional beta parameter $\overline{\beta} = \beta L^2/V$, which is, in fact, the inverse equatorial Rossby number. We should emphasize that, unlike the traditional equatorial scaling, which uses the equatorial deformation radius $L_d = (gH)^{\frac{1}{4}}/\beta^{\frac{1}{2}}$, the spatial scale is not rigidly related to other parameters here. If we suppose that

$$\lambda \to 0, \text{ and } \frac{gH\lambda}{V^2} = \mathcal{O}(1), \tag{5}$$

which immediately gives $V \ll \sqrt{gH}$, that is the characteristic velocity is much smaller than the phase velocity of the fastest waves $c = \sqrt{gH}$, like Kelvin wave, then the momentum and mass conservation equations become:

$$\partial_t \mathbf{v} + \mathbf{v} \cdot \nabla \mathbf{v} + \overline{\beta} y \, \hat{\mathbf{z}} \wedge \mathbf{v} + \nabla \eta = 0 \,, \tag{6}$$

$$\lambda(\partial_t \eta + \mathbf{v} \cdot \nabla \eta) + (1 + \lambda \eta) \, \nabla \cdot \mathbf{v} = 0. \tag{7}$$

In the leading order of the expansion in λ: $\mathbf{v} = \mathbf{v}_0 + \lambda \mathbf{v}_1 + ...$ equation (7) gives $\nabla \cdot \mathbf{v}_0 = 0$, and the motion is divergenceless. Hence, we can introduce a streamfunction for the leading-order velocity:

$$u_0 = -\partial_y \psi, \; v_0 = \partial_x \psi. \tag{8}$$

First-order corrections u_1, v_1 can be found in the next order of the asymptotic expansion in λ. There is no guarantee that such expansion converges, but numerical results presented below suggest that there is indeed a correspondence between solutions of the full equations (1), (2) and the asymptotic ones. Cross-differentiation of the zonal and meridional momentum equations allows to eliminate η and gives the vorticity equation for streamfunction:

$$\nabla^2 \psi_t + \mathcal{J}(\psi, \nabla^2 \psi) + \overline{\beta} \psi_x = 0, \tag{9}$$

where $\mathcal{J}$ denotes the Jacobian.

If topography would be of the order one, and would be kept, we would have $(H - b)u_0 = -\partial_y \psi$, $(H - b)v_0 = \partial_x \psi$ instead of (8), and the resulting system would become an equatorial version of the long-wave approximation, which is used for studies of the dynamical effects of topography in oceanography, cf. (Gill 1982). Here we will use it first without topography, in order to construct the modon solutions.

2.1.2. *One-layer RSW modons*

Equation (9) coincides with the infinite deformation radius limit of one-layer QG equation, e.g. Zeitlin (2018), so the construction of the modon solutions can be straightforwardly transposed, following the pioneering paper of Larichev and Reznik (1976). Let us recall that these solutions are obtained under hypothesis of steady motion with constant zonal velocity U, by supposing a linear relationship between the absolute vorticity and streamfunction in the co-moving frame, which leads to an inhomogeneous Helmholtz equation. It is solved by separation of variables in polar coordinates in terms of Bessel functions, first in the outer with respect to a separatrix domain, under condition of decay at infinity, and then in the inner domain, and matching the inner and outer solutions at the separatrix. The separatrix is a circle of radius a in the (x, y) - plane. The matching conditions are continuity of the

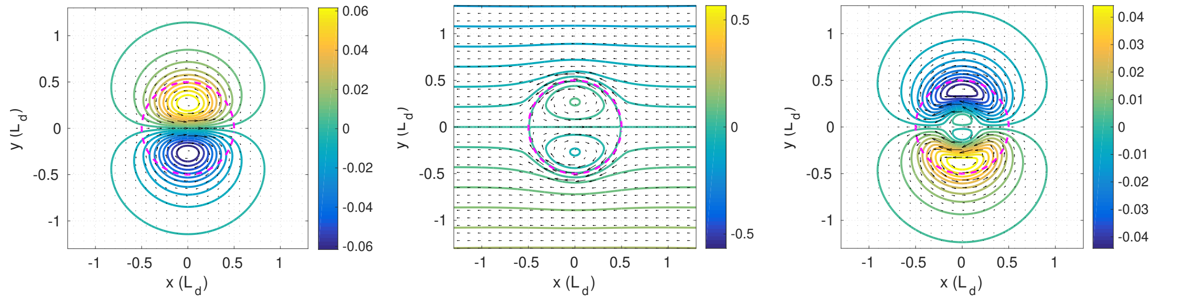

Figure 1. Streamlines and velocity field of the asymptotic modon corresponding to the first root $(a, p) = (0.5, 3.1623)$ of the equation (11), with slow eastward propagation $U = 0.1$, in stationary (*left panel*), and co-moving frames (*middle panel*), and a solution corresponding to the second root in the stationary frame (*right panel*). Dashed line: separatrix of radius a.

streamfunction and its normal derivative across the circle. It is worth noting that the actual size of the vortex, as a nonlinear solution, is larger than a. The solution is:

$$\begin{cases} \psi_{ext} = -\frac{Ua}{K_1(pa)} K_1(pr) \sin\theta, \quad r > a, \\ \\ \psi_{int} = \left[\frac{Up^2}{k^2 J_1(ka)} J_1(kr) - \frac{r}{k^2}(1 + U + Uk^2)\right] \sin\theta, \quad r < a, \end{cases} \tag{10}$$

where J_1 and K_1 are ordinary and modified Bessel functions, respectively, p is real, and $p^2 = \overline{\beta}/U$, so $U > 0$, and the motion is *eastward*. The matching conditions give:

$$\frac{J_1'(ka)}{J_1(ka)} = \frac{1}{ka}(1 + \frac{k^2}{p^2}) - \frac{k}{p}\frac{K_1'(pa)}{K_1(pa)}, \tag{11}$$

and for each pair (a, p) (or (a, U)) there exist a series of eigenvalues of k arising from (11), of which the lowest corresponds to a vortex dipole, to be called the asymptotic modon. We will be using below U as a governing parameter. The higher eigenvalues correspond to multi-polar vortices with significant velocity shear inside the core, which are more sensitive to dissipation, and are rarely considered in the literature. By construction, thus obtained solutions can be centered anywhere in the equatorial beta-plane. Yet it is only when the center of the circle is at the equator that the modon is a pair of cyclones, due to the change of sign of the planetary vorticity βy, otherwise it is a cyclone-anticyclone pair. The streamlines of the asymptotic modons corresponding to the first and the second roots of the equation (11) are presented in Fig. 1. Pressure distribution at a given ψ is obtained by differentiating and combining the leading-order momentum equations:

$$\nabla^2\eta = Hess[\psi] + \overline{\beta}(\psi_y + y\nabla^2\psi) \tag{12}$$

where $Hess[\psi] = \partial^2_{xx}\psi\, \partial^2_{yy}\psi - (\partial^2_{xy}\psi)^2$ is the Hessian of ψ. Notice that equations (9) and (12) are shallow-water counterparts of the non-divergent model for large-scale tropical motions derived in Charney (1963).

2.2. *Two-layer configuration*

2.2.1. *The model, and small pressure perturbation limit(s)*

We start with the “dry” two-layer atmospheric RSW momentum and mass equations in the equatorial β-plane with no topography and dissipation. The model is sketched in Figure

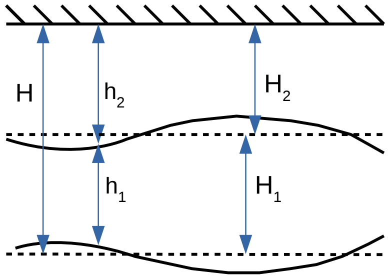

Figure 2. A sketch of the two-layer atmospheric rotating shallow water model.

2 The equations of the model read:

$$
\begin{cases}
\partial_t \mathbf{v_1} + \mathbf{v_1}\cdot\nabla\mathbf{v}_1 + \beta\, y\, \hat{\mathbf{z}}\wedge\mathbf{v}_1 + g\nabla(h_1+h_2) = 0\,,\\[2ex]
\partial_t \mathbf{v_2} + \mathbf{v_2}\cdot\nabla\mathbf{v}_2 + \beta\, y\, \hat{\mathbf{z}}\wedge\mathbf{v}_2 + g\nabla(h_1+sh_2) = 0\,,\\[2ex]
\partial_t h_1 + \nabla\cdot(\mathbf{v}_1 h_1) = 0\,,\\[2ex]
\partial_t h_2 + \nabla\cdot(\mathbf{v}_2 h_2) = 0\,,
\end{cases}
\tag{13}
$$

where $s = \theta_2/\theta_1 > 1$ is a stratification parameter, $\theta_{1,2}$ are potential temperatures of the layers, and β is the meridional gradient of the Coriolis parameter, as before. We introduce the deviations η_1 and η_2 of the free surface and interface between the layers from their positions at rest, respectively, and corresponding nonlinearity parameters $\lambda_{1,2}$, as follows:

$$
\begin{cases}
h_2 = H_2 - \eta_2 = H(d_2 - \lambda_2\overline{\eta}_2),\\[2ex]
h_1 = H_1 - \eta_1 + \eta_2 = H(d_1 - \lambda_1\overline{\eta}_1 + \lambda_2\overline{\eta}_2),
\end{cases}
\tag{14}
$$

Here $d_2 = H_2/H$, and $d_1 = H_1/H$ are non-dimensional thicknesses of the layers. d_1 and $d_2 = 1 - d_1$ are not independent. We nonetheless use both d_1 and d_2 explicitly in the formulas below to keep their expression concise. With the same choice of scaling as in the one-layer model for both layers, the non-dimensional equations (13) are:

$$
\begin{cases}
\partial_t \mathbf{v_1} + \mathbf{v_1}\cdot\nabla\mathbf{v}_1 + \overline{\beta}\, y\, \hat{\mathbf{z}}\wedge\mathbf{v}_1 = -\dfrac{gH\lambda_1}{V^2}\nabla\overline{\eta}_1,\\[2ex]
\partial_t \mathbf{v_2} + \mathbf{v_2}\cdot\nabla\mathbf{v}_2 + \overline{\beta}\, y\, \hat{\mathbf{z}}\wedge\mathbf{v}_2 = -\dfrac{gH}{V^2}[\lambda_1\nabla\overline{\eta}_1 - (1-s)\lambda_2\nabla\overline{\eta}_2],\\[2ex]
d_1\nabla\cdot\mathbf{v}_1 - \lambda_1[\partial_t\overline{\eta}_1 + \nabla(\overline{\eta}_1\mathbf{v}_1)] + \lambda_2[\partial_t\overline{\eta}_2 + \nabla(\overline{\eta}_2\mathbf{v}_1)] = 0,\\[2ex]
d_2\nabla\cdot\mathbf{v}_2 - \lambda_2[\partial_t\overline{\eta}_2 + \nabla(\overline{\eta}_2\mathbf{v}_2)] = 0,
\end{cases}
\tag{15}
$$

Even if we suppose that parameters s and $d_{1,2}$ which control the stratification are of the order one, there are still two small parameters $\lambda_{1,2}$ in the small pressure perturbations limit, and their ratio should be prescribed in order to fix a dynamical regime. There are two obvious choices: both λ_1 and λ_2 are of the same order, or one of them is much smaller than the other one. We will call them, respectively, Regime 1 and Regime 2, the second one having two sub-regimes depending on which of $\lambda_{1,2}$ is smaller.

2.2.2. *Regime 1*

In this regime deviations of the free surface and of the interface are of the same order: $\lambda_1 \sim \lambda_2 \sim \lambda \to 0$, hence $[(gH\lambda)/V^2] \sim 1$ and from the third and forth equations in (15) we get, analogously to the one-layer case: $\nabla \cdot \mathbf{v}_1 = \nabla \cdot \mathbf{v}_2 = 0$. Therefore,

$$\nabla^2 \psi_{(1,2)t} + \mathcal{J}(\psi_{(1,2)}, \nabla^2 \psi_{(1,2)}) + \overline{\beta} \psi_{(1,2)x} = 0, \tag{16}$$

where $\psi_{(1,2)}$ are streamfunctions in respective layers. Each of these equations has modon solutions, but they are not necessarily the same and may differ in scale and/or intensity. To the leading order, thus, the velocities in the layers do not influence each other, but the pressures do. Indeed, by taking divergence of the momentum equation for layer 1, and using the fact that to the leading order the divergence of velocity is zero, we get a diagnostic equation for η_1 analogous to (12), which allows to determine η_1 in terms of velocity in layer 1. Similar manipulations with the momentum equation for layer 2 give a diagnostic equation for η_2 which, however, contains η_1, and thus is taking into account a coupling between the layers. We should emphasize that the present dynamical regime is fully consistent with the construction of Charney (1963) for continuously stratified atmosphere, where the horizontal velocity obeying the equation (9) could have arbitrary modulation in the vertical.

2.2.3. *Regime 2a*

In this regime the deviation of the free surface is much smaller than that of the interface: $\lambda_1 \sim \lambda^2$, $\lambda_2 \sim \lambda \to 0$. Still supposing that $[(gH\lambda)/V^2] \sim 1$, we therefore have to rescale the lower-layer velocity: $\mathbf{v}_1 = \lambda \mathbf{v}_1^*$, and thus get:

$$\partial_t \mathbf{v_1^*} + \lambda \mathbf{v_1^*} \cdot \nabla \mathbf{v}_1^* + \overline{\beta}\, y\, \hat{\mathbf{z}} \wedge \mathbf{v}_1^* = -\nabla \overline{\eta}_1, \tag{17a}$$

$$\partial_t \mathbf{v_2} + \mathbf{v_2} \cdot \nabla \mathbf{v}_2 + \overline{\beta}\, y\, \hat{\mathbf{z}} \wedge \mathbf{v}_2 = (1-s)\nabla \overline{\eta}_2, \tag{17b}$$

$$d_1 \nabla \cdot \mathbf{v}_1^* + \partial_t \overline{\eta}_2 = 0, \tag{17c}$$

$$\nabla \cdot \mathbf{v}_2 = 0, \tag{17d}$$

Cross-differentiation and differentiation of (17a) give, respectively, to the leading order n λ:

$$\partial_t \zeta_1^* + \overline{\beta}\, y\, \nabla \cdot \mathbf{v}_1^* + \overline{\beta}\, v_1^* = 0, \tag{18a}$$

$$\partial_t (\nabla \cdot \mathbf{v}_1^*) - \overline{\beta}\, y\, \zeta_1^* + \overline{\beta}\, u_1^* = \nabla^2 \overline{\eta}_1, \tag{18b}$$

We introduce a potential and a streamfunction for the lower-layer velocity, which is not divergenceless, contrary to Regime 1:

$$\begin{cases} u_1^* = \phi_{1x}^* - \psi_{1y}^*, \\ v_1^* = \phi_{1y}^* - \psi_{1x}^*, \end{cases} \tag{19}$$

such that $\zeta_1^* = \nabla^2 \psi_1^*$ and $\nabla \cdot \mathbf{v}_1^* = \nabla^2 \phi_1^*$. Consequently Eq.(17c) can be rewritten as $\nabla^2 \phi_1^* = -(1/d_1)\eta_{2t}$. Substitution in (18a) gives:

$$\nabla^2 \psi_{1t} + \overline{\beta}\, \psi_{1x} = \frac{1}{d_1}(\overline{\beta}\, y \eta_{2t} + \partial_y \nabla^{-2} \eta_{2t}) \tag{20}$$

At the same time, the upper-layer equations (17b), (17d) have the same form as in the one-layer case, modulo a constant in front of the pressure gradient in the momentum equation, and are treated analogously giving equation (9) for the upper-layer streamfunction, which has asymptotic modon solutions. Equation (20) means that the equatorial modon in the upper layer is accompanied by a linear Rossby-wave field in the lower layer, which is forced by the pressure perturbations of the upper layer. Thus, the upper-layer modon is "leaky" and loses energy through the generation of this Rossby-wave field, which means that its coherence cannot be maintained for long time.

2.2.4. *Regime 2b*

In this regime the deviation of the interface is much smaller than that of the free surface $\lambda_1 \sim \lambda$, $\lambda_2 \sim \lambda^2$, which means that we have an effectively barotropic situation. Indeed, the equations for upper- and lower-layer velocities become identical in the leading order in λ:

$$\begin{cases} \partial_t \mathbf{v_1} + \mathbf{v_1} \cdot \nabla \mathbf{v}_1 + \overline{\beta}\, y\, \hat{\mathbf{z}} \wedge \mathbf{v}_1 = -\dfrac{gH\lambda}{V^2} \nabla \overline{\eta}_1, \\ \partial_t \mathbf{v_2} + \mathbf{v_2} \cdot \nabla \mathbf{v}_2 + \overline{\beta}\, y\, \hat{\mathbf{z}} \wedge \mathbf{v}_2 = -\dfrac{gH\lambda}{V^2} \nabla \overline{\eta}_1, \\ \nabla \cdot \mathbf{v}_1 = 0, \\ \nabla \cdot \mathbf{v}_2 = 0. \end{cases} \tag{21}$$

Hence $\mathbf{v}_1 = \mathbf{v}_2$ and we get an asymptotic modon solution which is uniform through the whole fluid column, that is barotropic, and the situation is effectively equivalent to the one-layer case.

3. Numerical simulations with asymptotic modon initializations in one- and two- layer RSW models

3.1. *Equatorial modon in different environments in one-layer model*

Numerical simulations in the one-layer case were performed in a symmetric with respect to the equator and wide enough domain, $9L_d \times 6.5L_d$, to minimize the boundary effects. Numerical sponges allowing to absorb short inertia-gravity waves were implemented at the boundaries. Here L_d is the equatorial deformation radius, $\sqrt{c/\beta}$, where $c = \sqrt{gH}$. We use the high-resolution, well-balanced finite-volume numerical scheme of Bouchut (2007). The dimensional units of length and time in the numerical scheme were L_d and $1/(\beta L_d)$, respectively, which corresponds to non-dimensional β equal to one. Dimensional values of g and β were fixed to be those for the Earth, thus the mean depth H is a single parameter. If, for example, it is chosen to be $H = 10km$, which roughly corresponds to two thirds of the thickness of the tropical troposphere, then the dimensional space and time units are $L_d \approx 3000km$, $1/\beta L_d \approx 3h$. Spatial resolution varied from 600×600 to 1200×1200, in order to check numerical convergence. No external forcing nor dissipation or thermal relaxation were introduced.

3.1.1. *Adjustment of asymptotic modons, and formation of RSW modons*

We first recall the results of the numerical simulations initialized with theoretical asymptotic modon solutions, which were sketched in Rostami and Zeitlin (2019a), and give some additional important details. The "dry" adiabatic RSW model is initialized with just a velocity field acquired from the asymptotic modon solution (10), with $U \ll \sqrt{gH}$, and no pressure perturbation. Nonlinear evolution of asymptotic modon leads to a process of relaxation presented in Fig. 3, which consists in emission of short inertia-gravity waves and formation of a dipolar coherent structure. Such "ageostrophic adjustment" of asymptotic modon to "real" modon solutions of the full RSW equations was first observed in the simulations with RSW model in the f-plane approximation in Ribstein et al. (2010). It lasts about one inertial period $T = 1/(\beta L_d)$. After adjustment of pressure and velocity fields to twin cyclones on both sides of the Equator, this coherent structure moves eastward, cf. Fig. 3. The phase speed of the modon depends on the values of (a, U) used for initialization. We compared the evolution starting from two sets of initial conditions corresponding to $U = 0.1$, $U = 0.2$ in (10), (11), both with radius $a = 0.5L_d$. We should emphasize that there is a threshold $U \approx 0.07$ be-

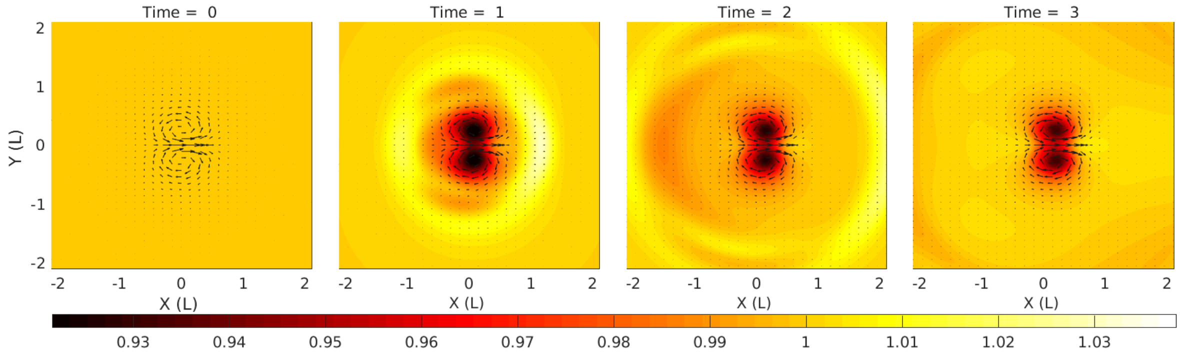

Figure 3. Initial "ageostrophic" adjustment of the asymptotic modon with parameters $(a, p) = (0.5, 3.1623)$ corresponding to initialization with an asymptotic modon with $U = 0.1$, as seen in the thickness field.

low which a coherent dipole does not form from the initialization with respective asymptotic modon. In both cases we have a formation of a coherent dipolar structure from the asymptotic modon. However, while the weaker/slower dipole corresponding to $U = 0.1$ eventually slows down and disaggregates at a distance $\approx 2\,L_d$ from the initial location, the stronger one with $U = 0.2$ continues to move eastward for much longer times. A comparison of the structure of the dipoles arising from each initialization is presented in Fig. 4, their coherence following from the scatter plot of potential vorticity vs Bernoulli function, cf. the left panel of Fig. 6. The resulting RSW modons differ essentially from the parent asymptotic ones, as they has a considerable thickness anomalies, cf. Fig. 4, with the respective values of non-dimensional nonlinearity parameter ≈ 0.075 and ≈ 0.15, respectively, but also a pronounced divergence pattern, as follows from Fig. 5.

In spite of their coherence, we detected an enstrophy loss during the propagation of thus arising RSW modons, which diminishes with increasing resolution (Fig. 6). This loss of enstrophy because of numerical dissipation, which also affects the energy conservation, is not negligible for weaker/slower modon ($U = 0.1, a = 0.5L_d$), while it is reduced to just few % for stronger/faster modons ($U = 0.2, a = 0.5L_d$).

3.1.2. *Modons in adiabatic vs most-convective environment*

We now switch on the effects of moisture within the simplest version of the diabatic moist-convective RSW (mcRSW) (Bouchut et al. 2009), in order to compare the behavior of equatorial modons in adiabatic and moist-convective environments. The equations of the model read:

$$\begin{cases} \partial_t \mathbf{v} + \mathbf{v}\cdot\nabla\mathbf{v} + \beta\, y\,\hat{\mathbf{z}}\wedge\mathbf{v} = -g\nabla h, \\ \partial_t h + \nabla\cdot(\mathbf{v}h) = -\gamma P, \\ \partial_t Q + \nabla\cdot(Q\mathbf{v}) = -P + E. \end{cases} \tag{22}$$

We introduced Q, a bulk amount of water vapor in the air column, with a condensation sink P and evaporation source E, which are parameterized as follows:

$$P = \frac{Q - Q^s}{\tau}\mathcal{H}(Q - Q^s), \quad E = \alpha|\mathbf{v}|(Q^s - Q)\mathcal{H}(Q^s - Q). \tag{23}$$

Here Q_s is a saturation moisture threshold, τ is relaxation time, α is a parameter regulating evaporation, γ is a parameter depending on background stratification, and $\mathcal{H}(...)$ denotes the Heaviside (step-)function. The parameterization of the condensation (23) is a bulk version of the Betts-Miller parameterization, and the parameterization of the evaporation is standard. As in the previous test simulations (Bouchut et al. 2009), we take a uniform initial moisture

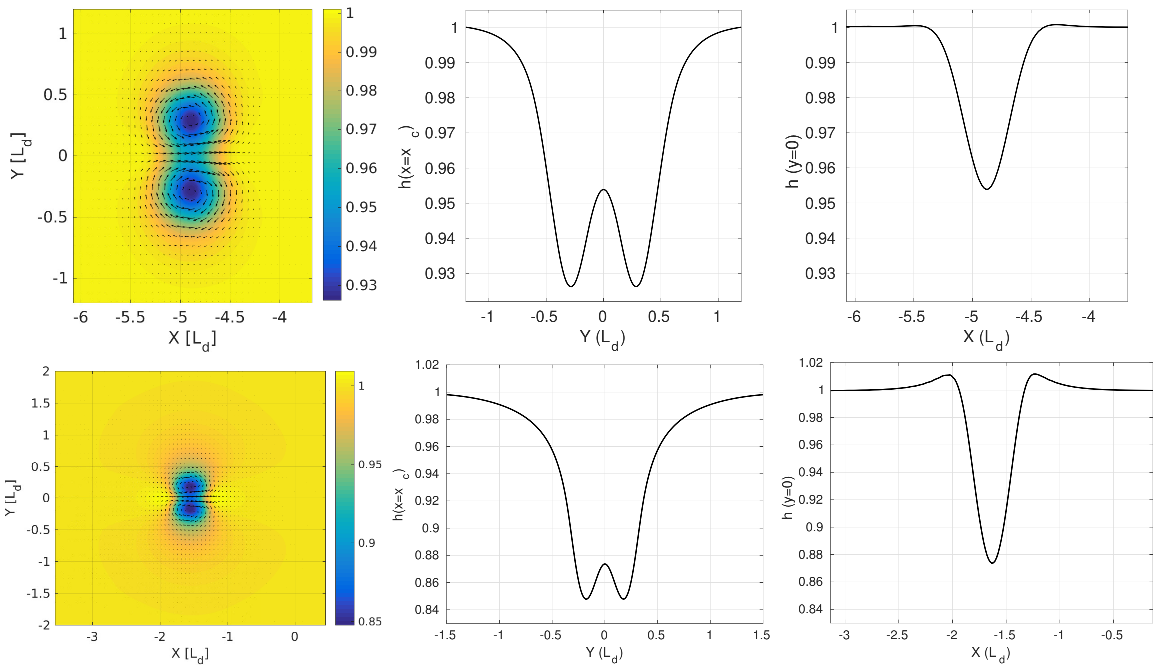

Figure 4. Comparison of the structure of weaker (*upper panel*) and stronger (*lower panel*) modons, arising, respectively from initializations with $U = 0.1$ and $U = 0.2$. *Left panel:* thickness h at $T = 3[\beta L_d]^{-1}$. *Middle panel:* meridional section across the center of the modon. *Right panel:* zonal section of the equatorial modon across the center of each cyclone.

distribution Q_i close to saturation: $Q_i = Q_s - 0.01$ with $Q_s = 0.9$, a short relaxation time τ equal to several time-steps of the numerical scheme, $\gamma = 1$, and $\alpha = \mathcal{O}(10^{-1})$. The values of $Q_{i,s}$ are chosen to be the same as in (Bouchut et al. 2009) for benchmarking reasons; small variations around them do not change qualitatively the results. A step-by-step comparison of propagation of an equatorial modon in "dry" and moist-convective environments is presented in Fig. 7. As follows from the Figure, the phase velocity of the modon in "dry" environment is $\approx 0.025\, L_d^2\, \beta \approx 5m/s$, while in moist-convective environment it increases to $\approx 0.035\, L_d^2\, \beta \approx 12m/s$, and the modon keeps its coherence. This is the effect of increase of the cyclonic vorticity due to the moist convection, which is easy to understand within the mcRSW model, cf. Lambaerts et al. (2011a). It is worth emphasizing that the phase velocity of a weak modon is not constant because of enstrophy and energy losses due to numerical dissipation. This is an indication that external friction forces are able to kill such modon. Nevertheless, the convective enhancement and related increase of velocity allow the modon to run over $\approx 3L_d$, which would be enough to pass over Indian Ocean, for example. Its scale, its propagation speed, and associated convection patterns of this equatorial modon (cf. Rostami and Zeitlin (2019a)) indicate a possible relevance to the MJO events. A specific feature introduced by the steady zonal motion of equatorial modons is the mean zonal velocity which is induced in the equatorial belt, and which can be of importance in the context of super-rotation of planetary atmospheres. We present the zonally averaged velocity profile introduced by a modon, both in adiabatic and moist-convective environments, in Fig. 8.

3.1.3. *Interactions of equatorial modons with topography*

We now investigate interactions of equatorial modons with topography, and changes in convective patterns introduced by this latter. For this, we consider a simplest configuration with an infinite zonally localized meridional ridge with a Gaussian profile of height, which is situated downstream from the advancing modon. The maximum height of the ridge is $b_{\max} = 0.2H$ and it median width is equal to the radius of the core of the modon. The results are presented in Fig. 9. As seen in the Figure, the only effect of the ridge upon the

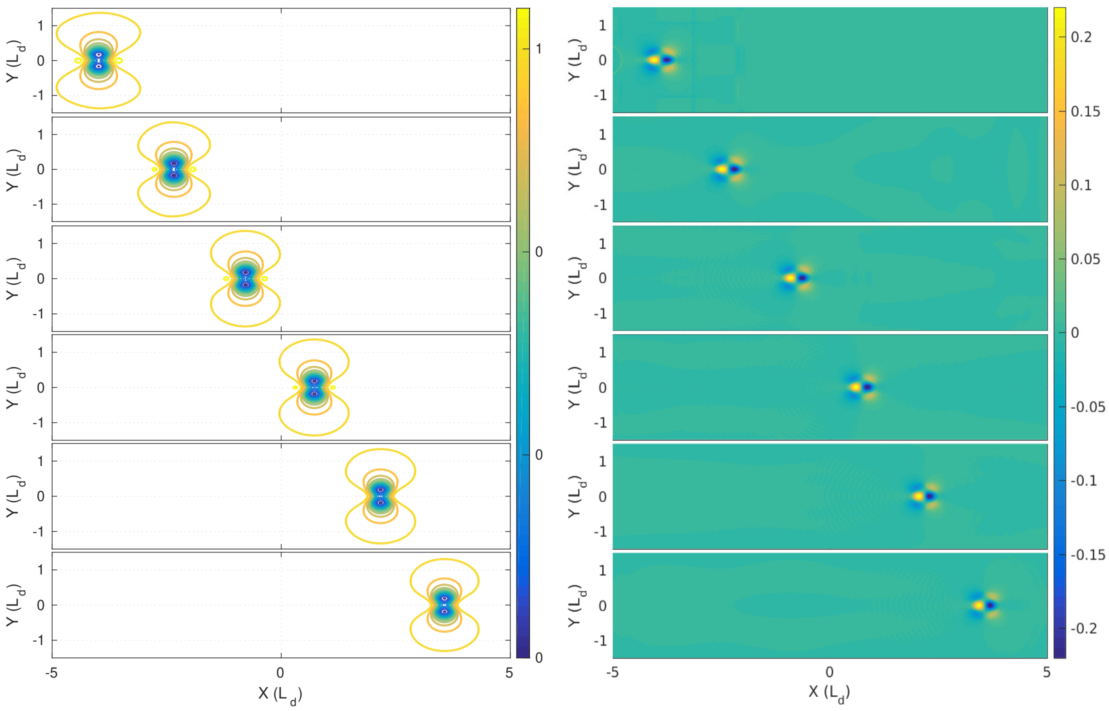

Figure 5. Snapshots at $T = 0, 10, 20, 30, 40, 50$ $[1/(\beta L_d)]$ after initial adjustment, from top to bottom, of h (*left panel*) and divergence (*right panel*) of the modon initialized with $a = 0.5, U = 0.2$.

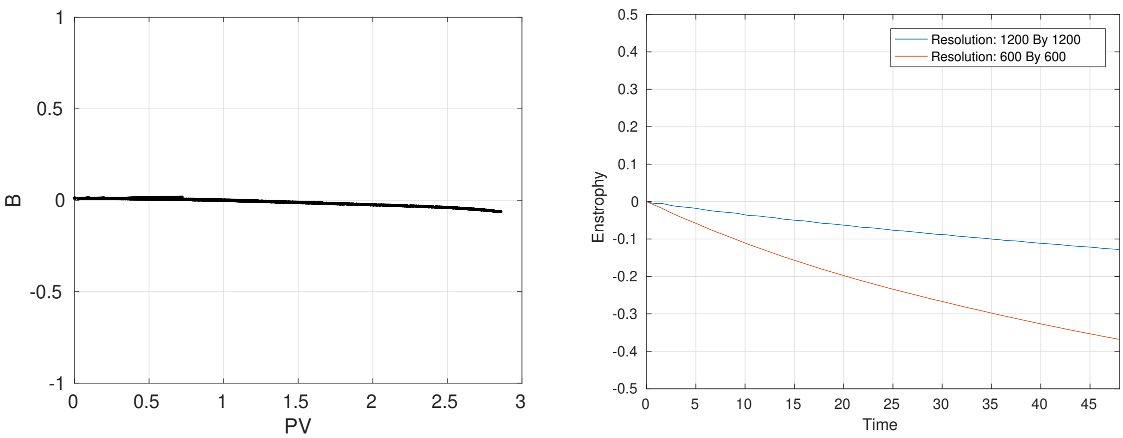

Figure 6. *Left panel*: Scatter plot of Bernoulli function (mean value subtracted) in the co-moving frame vs potential vorticity (PV), which demonstrates the coherence of the modon. initialized with $(a, p) = (0.5, 3.1623)$, corresponding to $U = 0.1$. *Right panel*: Sensitivity of the loss of enstrophy to numerical resolution.

geopotential and vorticity fields is a temporary lateral extension of the modon during the passage over the ridge, which does not change neither its trajectory, nor coherence. Yet, the zonal speed of the modon over topography abruptly decreases. Fig.10 shows evolution of divergence and condensation patterns associated with the modon during the passage over the ridge. Generation of inertia-gravity waves and of topographic waves, with related condensation patterns is clearly seen. A weak signal corresponding to a reflected Rossby wave can be identified on the left panel of Fig. 9, to the left of the ridge. Notice a typical condensation pattern associated with the modon far from topography, which resembles that of the MJO events.

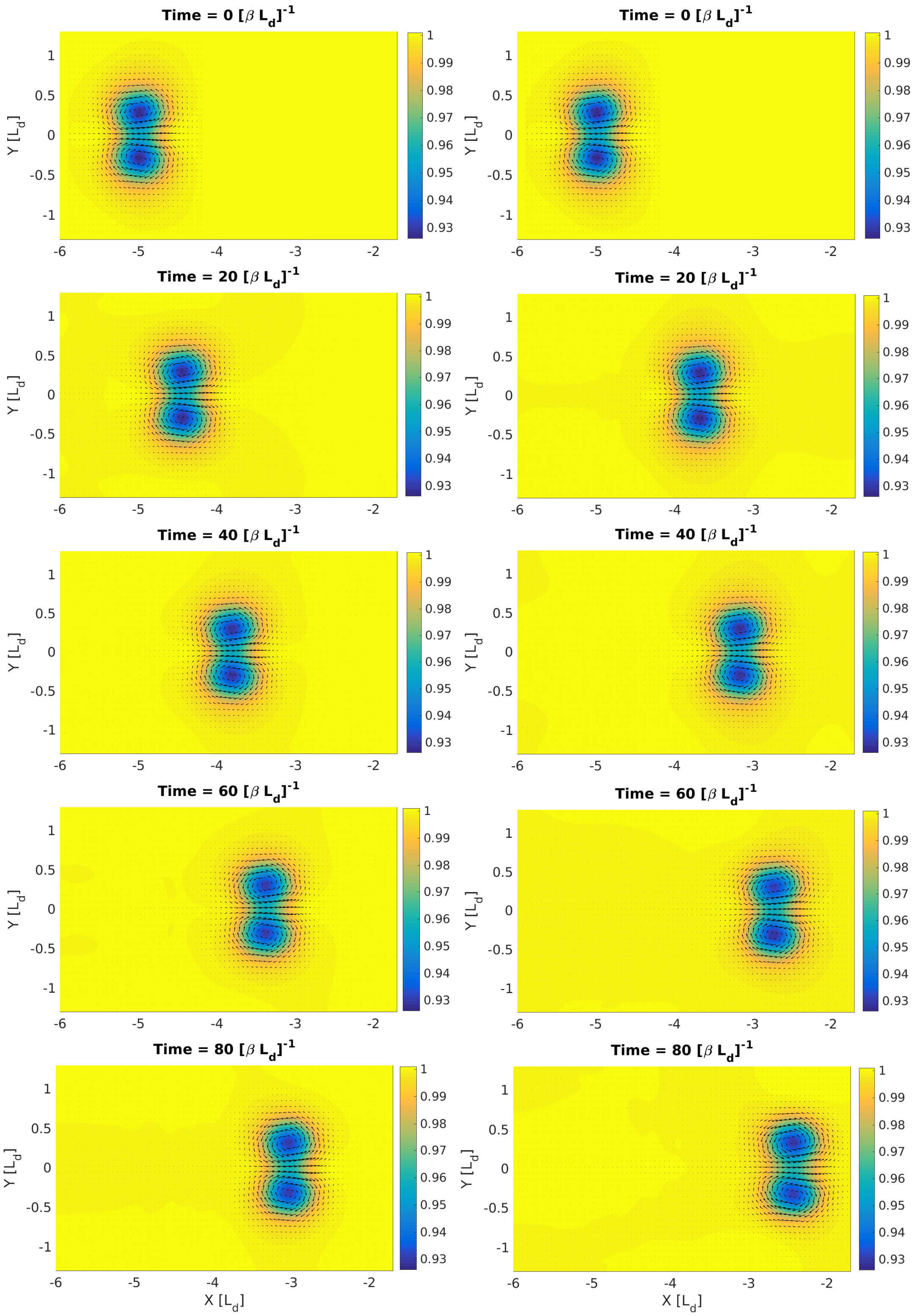

Figure 7. Snapshots of pressure and velocity fields of the modon arising from an asymptotic modon initialization with $U = 0.1$ ($(a, p) = (0.5, 3.1623)$) in adiabatic (*left panel*) and moist-convective (*right panel*) environments.

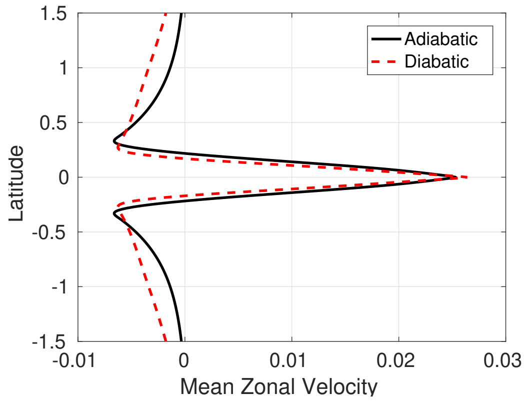

Figure 8. Superposition of steady-state mean zonal velocity profile induced by the modon initialized with $a = 0.5, U = 0.2, \beta = 1$ in adiabatic (*solid line*) and diabatic (*dashed line*) environments.

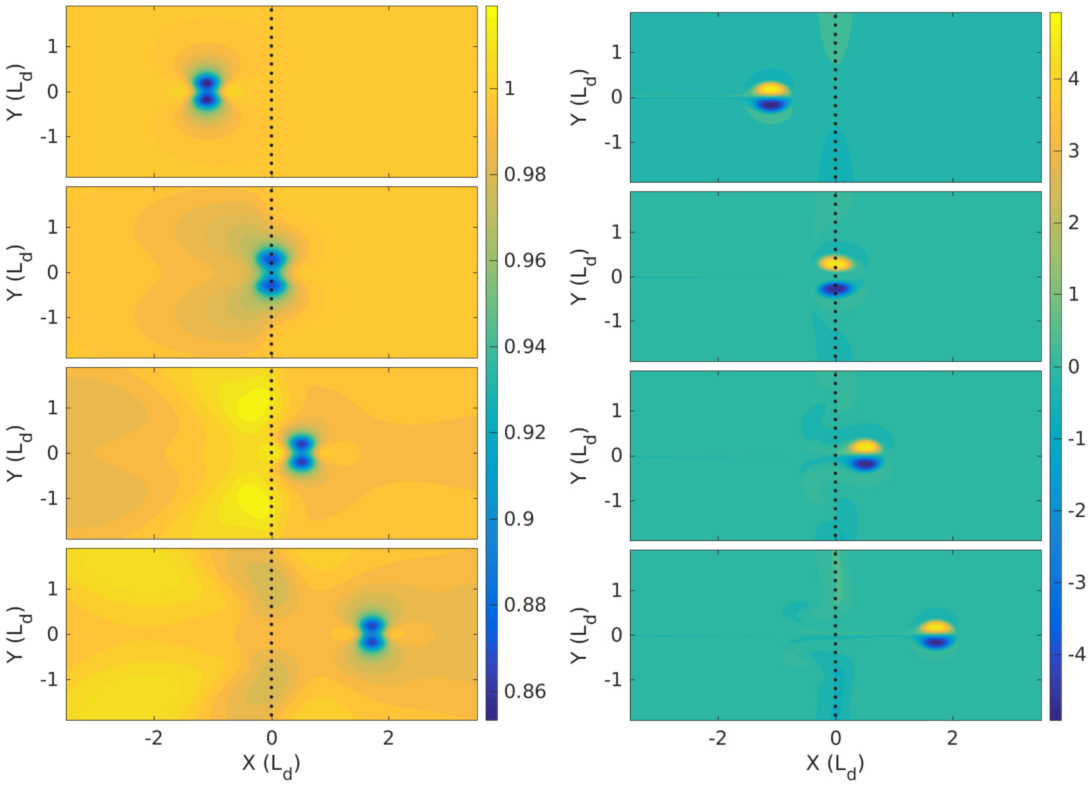

Figure 9. Propagation of the equatorial modon in moist-convective environment over an idealized meridional ridge of Gaussian shape, as seen in the geopotential height (*left column*) and relative vorticity (*right column*) fields. Snapshots at $T = 10, 20, 30, 40\ [1/(\beta L_d)]$, from top to bottom. Maximum height of the ridge is $0.2H$, and its median width is $[-0.25 \quad .25]$. Vertical dashed line represents the position of the center of the ridge. ($a = 0.5, U = 0.2, \alpha = 0.05$).

3.2. *Two-layer Equatorial Modons*

3.2.1. *Adjustment of asymptotic modons, and existence of two-layer shallow-water modons in adiabatic environment*

Following the strategy which proved to be fruitful in the one-layer model, and using the fact that the asymptotic modon solutions in Regimes 1 and 3 of section 2.2 are the same as in the one-layer model layerwise, we first initialize the simulations with "dry" two-layer equations (13) by the velocity field of the asymptotic modon solutions of section 2.1.2 in

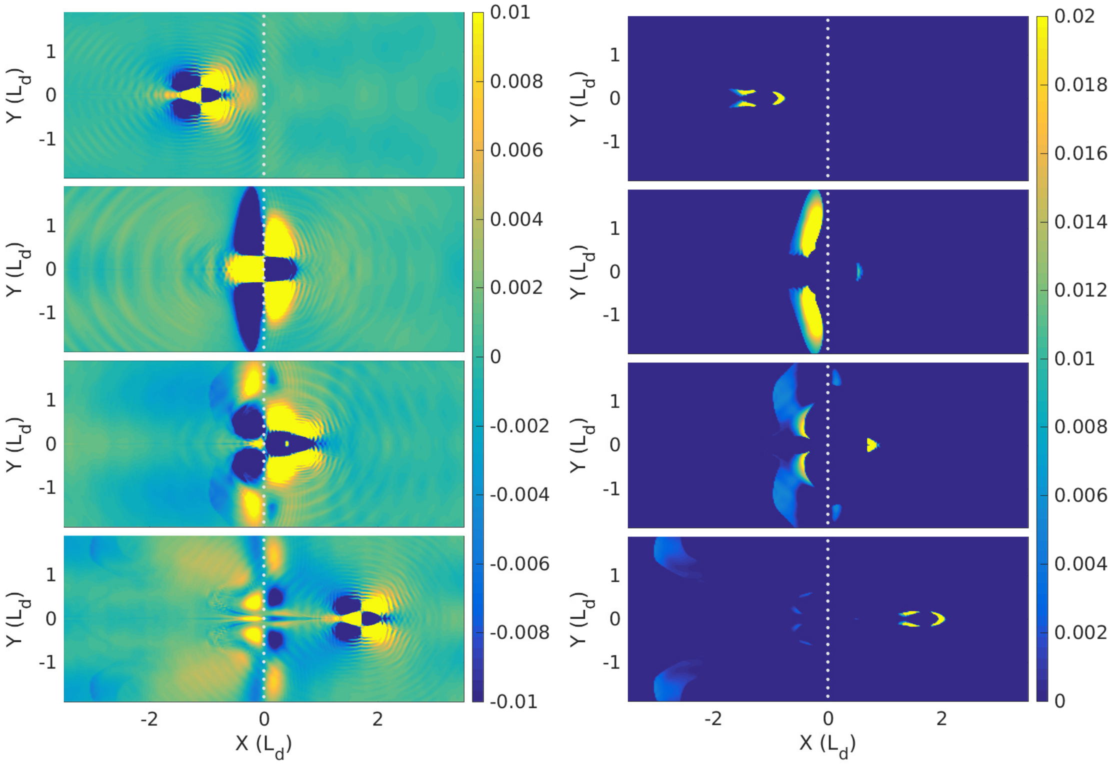

Figure 10. Evolution of divergence (*left column*) and condensed water vapor (*right column*) fields during the passage of an equatorial modon over an idealized meridional ridge in moist-convective environment. Snapshots at $T = 10, 20, 30, 40$ $[1/(\beta L_d)]$, from top to bottom. Same conventions as in Fig. 9.

each layer, and no pressure perturbations, with a hope that via the process of ageostrophic adjustment these configurations will end up in quasi-stationary states, like in the one-layer case. Notice that such initialization fits all the regimes of section 2.2, as pressure anomalies of the layers are initially identically zero. For simulations with two-layer model we are using the numerical scheme of Bouchut and Zeitlin (2010), which was successfully tested in numerous applications. In all simulations below the nonperturbed thicknesses of the layers are the same, with the same total thickness as in the one-layer case, and the stratification parameter s is equal to 1.1. The simulations were performed with initializations corresponding to asymptotic modons of different sizes and intensities in respective layers. The overall conclusion following from such experiments is that only the initializations with identical, or very close, asymptotic modons in each layer, i.e. quasi-barotropic initializations, give rise to coherent slowly eastward-propagating structures, while essentially baroclinic initializations are eventually transformed into equatorial Rossby-wave packets, although initially they form dipoles which may move eastwards for some time.

A comparison of the evolution of strictly barotropic and weakly baroclinic initializations with velocity fields corresponding, respectively, to the asymptotic modon of sec. 2.1.2 with $U_1 = U_2 = 0.2$ in both layers , and with $U_1 = 0.2$ in the lower, and $U_2 = 0.1$ in the upper layer is presented in Figure 11. As follows from the figure, the barotropic initialization leads to a barotropic coherent dipole keeping its form and moving eastwards, while the dipole produced by the weakly baroclinic initialization slows down and then engages in the reverse westward motion losing its shape at the same time, that is gradually becoming a packet of Rossby waves. The diagnostics of coherence with the scatter plots of Bernoulli function vs. PV in the lower layer presented in Figure 12 confirm this conclusion. In the following we will be calling stronger (weaker) baroclinic configurations those with larger (smaller) difference

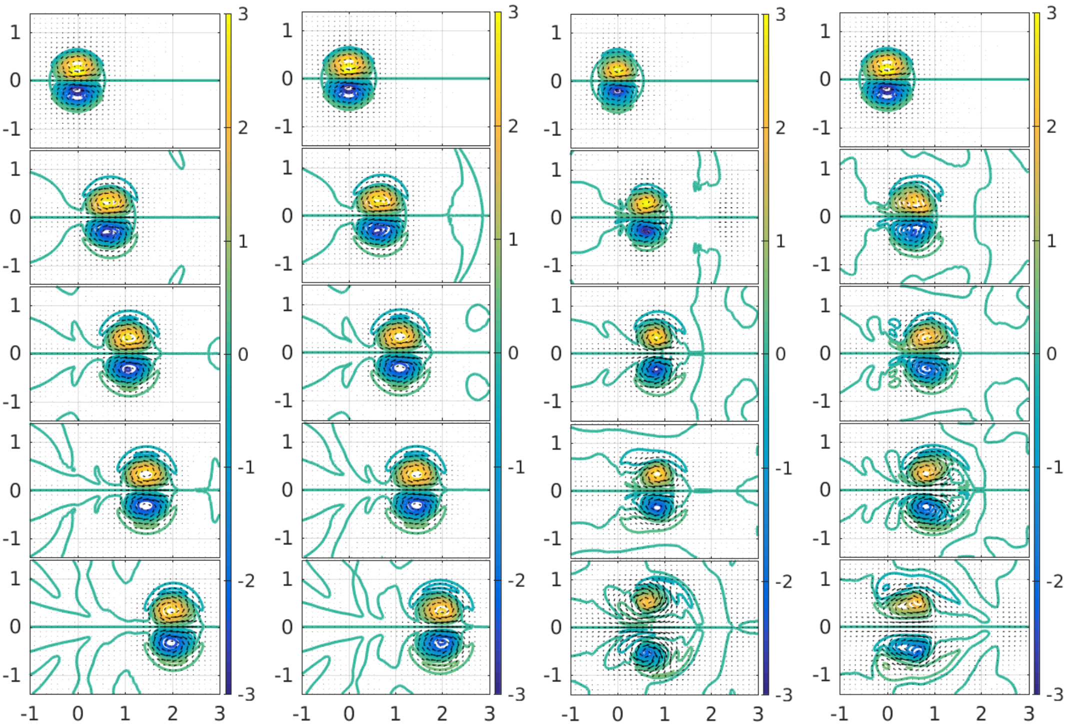

Figure 11. "Dry" evolution of relative vorticity layer-wise starting from barotropic (*first column: upper layer, second column: lower layer*) and weakly baroclinic (*third column: upper layer, fourth column: lower layer*) initializations with velocity fields corresponding, respectively, to the asymptotic modon of sec. 2.1.2 with $U_1 = U_2 = 0.2$ in both layers , and with $U_1 = 0.2$ in the lower, and $U_2 = 0.1$ in the upper layer. Snapshots at $T = 0, 10, 20, 30, 50$ $[1/(\beta L_d)]$, from top to bottom.

between the amplitudes of initial parameters of asymptotic-modon initializations in the layers $U_1 - U_2$. Our results show that strong baroclinic initializations do not produce coherent long-living dipoles. A comparison of the evolution of strongly baroclinic initializations, with asymptotic modon velocity parameter $U_2 = 0.2$ in the lower layer, with quiescent upper layer ($U_1 = 0$), and, inversely, with the same field in the upper layer, with quiescent lower layer is presented in Figure 13, and shows a similar, modulo the layer swap, behavior displaying a transformation of initial dipole into a wave-train. Analogous initialization with $U_1 = 0.1$, i.e. smaller baroclinicity, produces a more coherent and long-leaving structure, see Figure 14 below.

3.2.2. *2-layer modons in moist-convective environment*

To perform the two-layer simulations in moist-convective environment we work on the equatorial beta-plane with the simplest version of two-layer mcRSW with moist lower and dry upper layers, which was proposed in Lambaerts et al. (2011b) and ameliorated by including evaporation in Rostami and Zeitlin (2017). The equations of the model, in the same setting

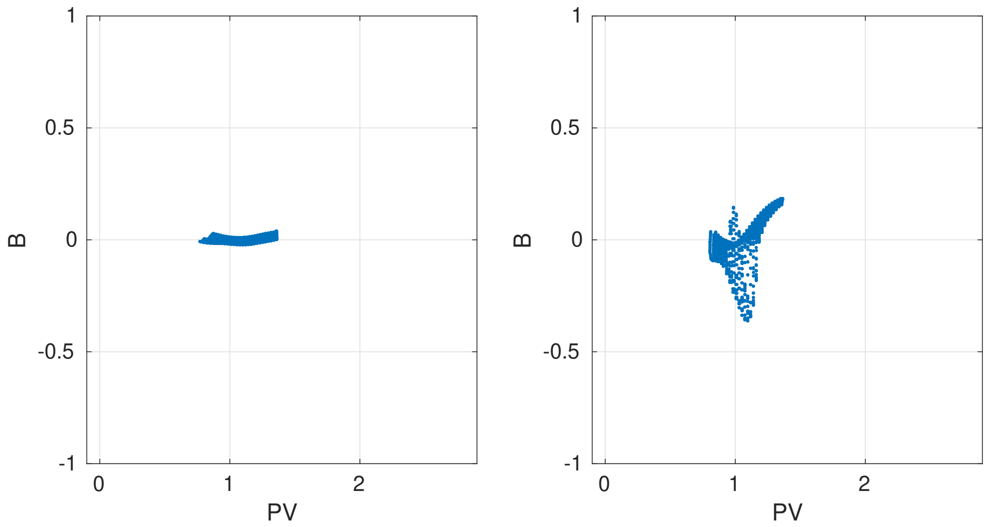

Figure 12. Comparison of scatter plots of Bernoulli function (with subtracted mean value) vs PV in the lower layer of barotropic (*left panel*), and baroclinic (*right panel*) dipoles of Fig. 11 ($U_1 = 0.2, U_2 = 0.1$) at $T = 20\,[1/(\beta L_d)]$, computed in a circle of radius $2a/3$ with respect to the center of the dipole.

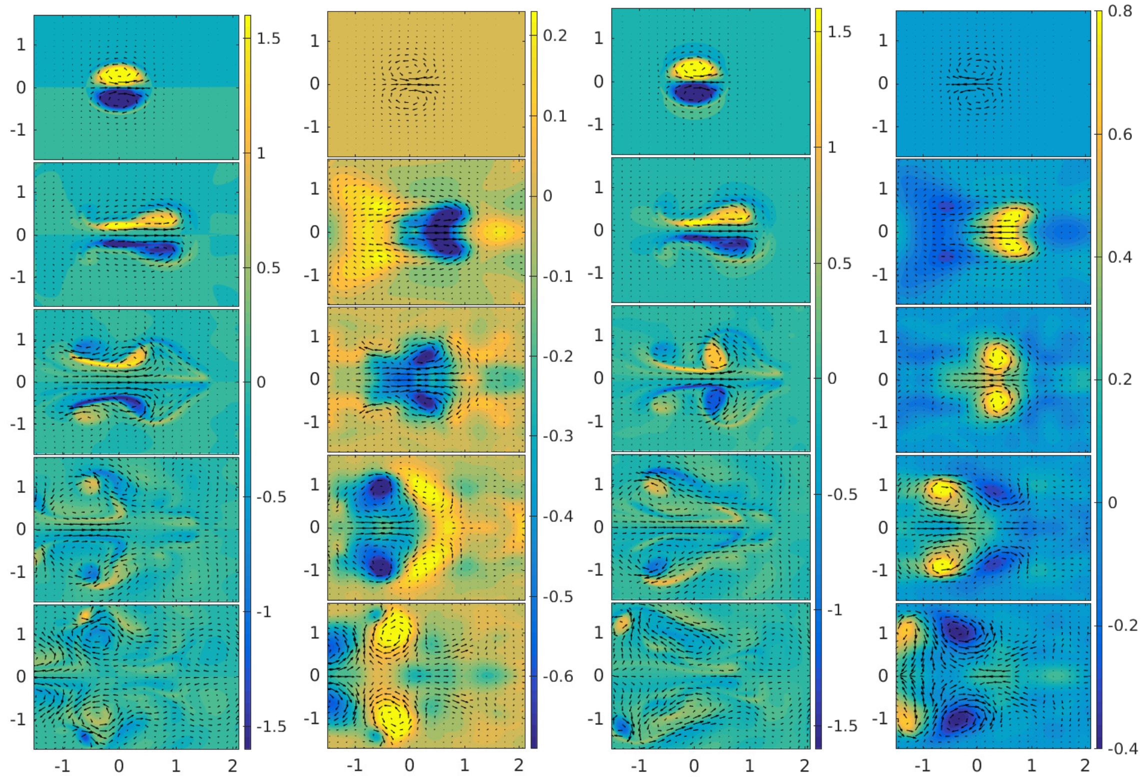

Figure 13. "Dry" evolution of relative vorticity in the lower layer (*first column*), and baroclinic velocity $\boldsymbol{v}_1 - \boldsymbol{v}_2$ and pressure $\eta_1 - \eta_2$ (*second column*) produced by essentially baroclinic initializations with the velocity parameter of the asymptotic modon of sec. 2.1.2 in the lower layer $U_1 = 0.2$, and quiescent upper layer: $U_2 = 0$. Same for initialization with asymptotic modon in the upper layer with $U_1 = 0, U_2 = 0.2$, respectively, the relative vorticity (*third column*), and baroclinic velocity and pressure (*fourth column*) in the upper layer. Snapshots at $T = 0, 15, 40, 60, 80$ $[1/(\beta L_d)]$, from top to bottom.

as in (13), read:

$$\begin{cases} \dfrac{D_1 \boldsymbol{v}_1}{Dt} + \beta y\, \hat{\mathbf{z}} \wedge \boldsymbol{v}_1 = -g\boldsymbol{\nabla}(h_1 + h_2), \\ \dfrac{D_2 \boldsymbol{v}_2}{Dt} + \beta y\, \hat{\mathbf{z}} \wedge \boldsymbol{v}_2 = -g\boldsymbol{\nabla}(h_1 + sh_2) + \dfrac{\boldsymbol{v}_1 - \boldsymbol{v}_2}{h_2}\beta P_1, \\ \dfrac{D_1 h_1}{Dt} + \boldsymbol{\nabla}\cdot(h_1 \boldsymbol{v}_1) = -\beta P_1, \\ \dfrac{D_2 h_2}{Dt} + \boldsymbol{\nabla}\cdot(h_2 \boldsymbol{v}_2) = +\beta P_1, \\ \partial_t Q_1 + \boldsymbol{\nabla}\cdot(Q_1 \boldsymbol{v}_1) = -P_1 + E. \end{cases} \tag{24}$$

Here $D_i/Dt = \partial_t + \boldsymbol{v}_i \cdot \boldsymbol{\nabla} \boldsymbol{v}_i$, $i = 1, 2$. The convective flux is linked to the water-vapour condensation P_1 in the lower, humid layer, and produces a sink (source) in the mass conservation equation in the lower (upper) layer, like in the one-layer mcRSW (22). However, now the total mass is conserved. Due to the convective mass exchange the same flux leads to appearance of the Rayleigh drag in the upper-layer momentum equation. Condensation and evaporation are expressed in terms of the bulk moisture in the lower-layer column Q_1 in the same way as in (23). The equations (22) arise from (24) in the limit of infinitely thick upper layer. The setup is the same as in the "dry" simulations above. We take a uniform initial moisture distribution in the lower layer close to saturation: $Q_1 = Q_s - 0.01$ with $Q_s = 0.8$, and choose $\alpha = 0.2$.

Before presenting the results of numerical experiments with two-layer mcRSW, let us recall that condensation leads to enhancement of cyclonic vorticity in moist-convective environment, as already mentioned. Hence, one can expect that, as in the one-layer case, the effects of condensation make the dipoles arising from the adjustment of asymptotic modons more robust. This is, indeed, what happens. In Figure 14 we show a comparison of "dry" and moist-convective evolution produced by the same as in Figure 13 initialization, but with a weaker baroclinicity, with $U_1 = 0.1$, and quiescent upper layer. As follows from the Figure, the "dry" modon in the lower layer keeps its coherence, while moving eastward for some time, but then changes shape and engages in a westward motion becoming a looser dipole. The moist-convective evolution, with the same initial perturbation, maintains the eastward motion and coherence of the initial modon in the lower layer for much longer times, with more intense cyclonic vorticity compared to the "dry" case, although, eventually, the dipole is getting looser and stops.

It would be tempting to interpret the westward-moving dipole arising in the "dry" scenario in Figure 14 as a Rossby-wave soliton discovered by Boyd (1985) (which was also called modon) and shown, theoretically and numerically, to arise in the equatorial adjustment of pressure perturbations in (LeSommer et al. 2004). However, the Boyd's soliton is expected to arise at much larger zonal to meridional aspect ratios, and was observed in numerical simulations in a form of *anticyclonic* dipole. In fact, although the cyclonic dipole we observe maintains its coherence for some time, it eventually loses it and becomes an equatorial Rossby-wave train (not shown).

An interesting result is obtained with the barotropic initialization corresponding to the case of Figure 11 in moist-convective environment. It is presented in Figure 15, and shows that while the arising modon maintains it coherence for a long time, as follows from the vorticity snapshots (not shown), its baroclinic pressure pattern exhibits a quadrupolar structure, similar to that observed in the MJO events (Zhang 2005), with the condensation pattern also resembling that of MJO.

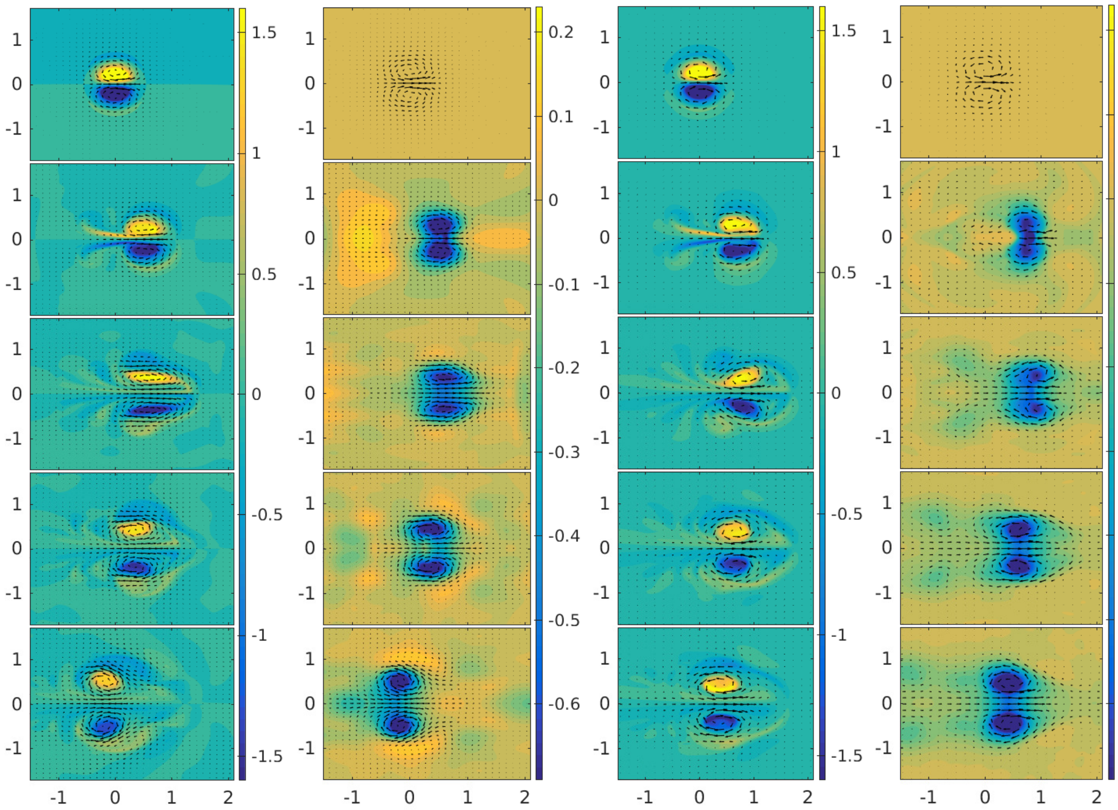

Figure 14. Comparison of "dry" (*first and second columns*) and moist-convective (*third and fourth columns*) evolution of relative vorticity in the lower layer (*first and third panels*), and baroclinic velocity $\boldsymbol{v}_1 - \boldsymbol{v}_2$ and pressure $\eta_1 - \eta_2$ (*second and fourth panels*) following an essentially baroclinic initialization with the velocity field in the lower layer corresponding to the asymptotic modon of sec. 2.1.2 with $U_1 = 0.1$, and quiescent upper layer: $U_2 = 0$. Snapshots at $T = 0, 15, 40, 60, 80$ $[1/(\beta L_d)]$, from top to bottom.

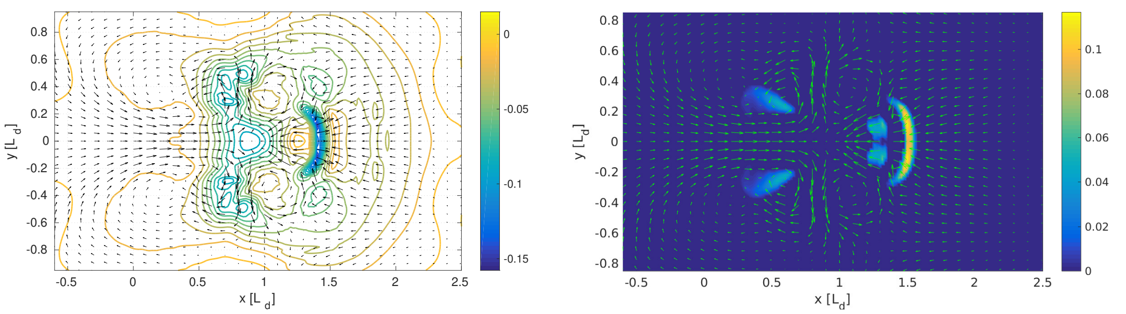

Figure 15. Snapshot at time at $T = 20$ $[1/(\beta L_d)]$ of baroclinic velocity $\boldsymbol{v}_1 - \boldsymbol{v}_2$ and pressure $\eta_1 - \eta_2$ (*left panel*) and condensation pattern (*right panel*) produced by barotropic initialization with the velocity field in both layers corresponding to the asymptotic modon of sec. 2.1.2 with $U = 0.2$.

4. Conclusion and Discussion

We, thus, established existence of nonlinear long-living, slow eastward-moving dipolar coherent structures, the modons, in the shallow-water dynamics in the equatorial beta-plane, both in one- and two-layer versions of the model, although robust modons are essentially barotropic in the latter case. These solutions of the fluid equations of motion at the Equator seem to be overlooked in the literature. The modons maintain their coherence in the presence of moisture and are accompanied by a specific and persistent moist convection patterns, if condensation and evaporation are included. The scales of these structures are conditioned by the interpretation of the RSW model. At given g and β the actual scales depend on the value of the unperturbed thickness H, or, equivalently, on the value of the corresponding deformation radius L_d. A crucial observation which put us on the track of equatorial modons is that Charney (1963) equation for equatorial balanced motions coincides with (9) modulo parametric dependence on the vertical coordinate. Therefore, solutions of Charney's balance equations in a form of asymptotic modons in the horizontal, with vertical modulation, do exist, although it remains to prove that they survive in the full primitive equations. As we showed, this is the case in one- and two-layer shallow-water models, provided the vertical modulation is weak.

Coming back to a possible relation to MJO, we should emphasize that some features detected in numerical simulations we presented are indeed in resemblance with the MJO events. These latter clearly display twin cyclonic structures in the lower layer (Rui and Wang 1990, Yanai et al. 2000, Adames et al. 2014), and a quadrupolar structure of the first baroclinic mode (Zhang 2005). An equivalent barotropic structure of MJO with a strong dipolar vorticity component was recently emphasized by Wang et al. (2019). Condensation/precipitation patterns associated with equatorial modons resemble those of dipolar structures related to MJO. Intensification and acceleration of the equatorial modons in moist-convective environment is consistent with the observation that the regions of most active MJO are correlated with the areas of large mean precipitation (Zhang and Dong 2004).

We should, however, say that, apparently, barotropic, or quasi-barotropic, modons alone are not sufficient to explain the MJO events in all their complexity. It should not be forgotten that these events do not maintain a fixed structure all the time, and have their own life-cycle, an important part of which is related to interactions with Kelvin waves, e.g. (Haertel et al. 2014). A coupling of a baroclinic long-living modon-like structure in the moist-convective environment, like that displayed in Figure 14, and a Kelvin wave, which was out of the scope of the present study, can be shown to play a primordial role in the MJO dynamics (Rostami and Zeitlin 2020). Yet, the coherent dipolar structures are certainly part of the MJO events, and the increase of their eastward velocity with increase of intensity of the moist convection is to be borne in mind in the context of global change and expected increase of temperature of the oceans.

The existence of the slowly eastward-moving equatorial modons, and the scenarios of their evolution, in particular in the presence of moist convection, should be not forgotten in data analyses both on the Earth and on other planets. For example, the classical Gill's mechanism (Gill 1980) was evoked in (Legarreta et al. 2016) with a support of "dry" RSW simulations, in order to explain the so-called Y-shaped structures observed in the equatorial atmosphere of Jupiter. The modifications of this mechanism with changes of parameters, and its ability to generate equatorial modons, which were reported in (Rostami and Zeitlin 2019b), and also the role of moist convection, which is known to be present in the Jovian atmosphere, as well as the above-described scenario of transformation of eastward-moving coherent dipoles into westward-moving and meridionally separating vortex pairs, should be kept in mind in this context.

References

Adames, A. F., Patoux, J., Foster, R. C., 2014. The contribution of extratropical waves to the MJO wind field. J. Atmos. Sci. 71 (1), 155–176.
Bouchut, F., 2007. Chapter 4: Efficient numerical finite volume schemes for shallow water models. In: Zeitlin, V. (Ed.), Nonlinear Dynamics of Rotating Shallow Water: Methods and Advances. Vol. 2 of Edited Series on Advances in Nonlinear Science and Complexity. Elsevier, pp. 189 – 256.
Bouchut, F., Lambaerts, J., Lapeyre, G., Zeitlin, V., 2009. Fronts and nonlinear waves in a simplified shallow-water model of the atmosphere with moisture and convection. Phys. Fluids 21 (11), 116604.
Bouchut, F., Zeitlin, V., 2010. A robust well-balanced scheme for multi-layer shallow water equations. Disc. Cont. Dyn. Sys. B 13 (4), 739–758.
Boyd, J., 1985. Equatorial solitary waves. Part 3. Westward traveling modons. J. Phys. Oceanogr. 15, 46–54.
Charney, J., 1963. A note on large-scale motions in the tropics. J. Atmos. Sci. 20, 607–609.
Gill, A., 1980. Some simple solutions for heat induced tropical circulation. Q. J. Roy. Met. Soc. 106, 447–462.
Gill, A., 1982. Atmosphere - Ocean Dynamics. Academic Press.
Haertel, P., Straub, K., Budsock, A., 2014. Transforming circumnavigating Kelvin waves that initiate and dissipate the Madden - Julian Oscillation. Q. J. Roy. Met. Soc. 141, 1586–1602.
Haertel, P., Straub, K., Fedorov, A., 2013. Lagrangian overturning and the Madden - Julian oscillation. Q. J. Roy. Met. Soc. 140, 1344–1361.
James, I., 1994. Introduction to Circulating Atmospheres. Cambridge University Press.
Kim, D., Sobel, A., Maloney, E., Frierson, D., Kang, I., 2011. A systematic relationship between intraseasonal variability and mean state bias in AGCM simulations. J. Climate 24, 5506–5520.
Kizner, Z., Reznik, G., Fridman, B., Khvoles, R., McWilliams, J., 2008. Shallow-water modons on the f - plane. J. Fluid Mech. 603, 305–329.
Lahaye, N., Zeitlin, V., 2016. Understanding instabilities of tropical cyclones and their evolution with a moist convective rotating shallow - water model. J. Atmos Sci. 73, 505–523.
Lambaerts, J., Lapeyre, G., Zeitlin, V., 2011a. Moist versus dry barotropic instability in a shallow water model of the atmosphere with moist convection. J. Atmos. Sci. 68, 1234–1252.
Lambaerts, J., Lapeyre, G., Zeitlin, V., Bouchut, F., 2011b. Simplified two-layer models of precipitating atmosphere and their properties. Phys. Fluids 23, 046603.
Larichev, V., Reznik, G., 1976. Two-dimensional solitary Rossby waves. Doklady USSR Acad. Sci. 231, 1077–1080.
Legarreta, J., Barrado-Izagirre, N., Garcia-Melendo, E., Sanchez-Lavega, A., Gomez-Forrellad, J., IOPW, 2016. A large active wave trapped in Jupiter's equator. A & A A15, A154.
LeSommer, J., Reznik, G., Zeitlin, V., 2004. Nonlinear geostrophic adjustment of long-wave disturbances in the shallow-water model on the equatorial beta-plane. J. Fluid Mech. 515, 135–170.
Madden, R., Julian, P., 1972. Description of global-scale circulation cells in the tropics with a 40-50 day period. J. Atmos. Sci. 29, 1109–1123.
Majda, A. J., Stechman, S. N., 2009. The skeleton of tropical intraseasonal oscillations. PNAS 106, 8417–8422.
Matsuno, T., 1966. Quasi-geostrophic motions in the equatorial area. J. Met. Soc. Japan 44, 25–43.
Ribstein, B., Gula, J., Zeitlin, V., 2010. (A)geostrophic adjustment of dipolar perturbations, formation of coherent structures and their properties, as follows from high-resolution numerical simulations with rotating shallow water model. Phys. Fluids 22, 116603.
Rostami, M., Zeitlin, V., 2017. Influence of condensation and latent heat release upon barotropic and baroclinic instabilities of vortices in a rotating shallow water f-plane model. Geophys. Astrophys. Fluid Dyn. 111 (1), 1–31.
Rostami, M., Zeitlin, V., 2018. Improved moist-convective rotating shallow water model and its application to instabilities of hurricane-like vortices. Q. J. Roy. Met. Soc. 144, 1450–1462.
Rostami, M., Zeitlin, V., 2019a. Eastward-moving convection-enhanced modons in shallow water in the equatorial tangent plane. Phys. Fluids 31, 021701.
Rostami, M., Zeitlin, V., 2019b. Geostrophic adjustment on the equatorial beta-plane revisited. Phys. Fluids 31, 081702.
Rostami, M., Zeitlin, V., 2020. Can geostrophic adjustment of baroclinic disturbances in tropical atmosphere explain MJO events? Q. J. Roy. Met. Soc. https://doi.org/10.1002/qj.3884.
Rui, H., Wang, B., 1990. Development characteristics and dynamical structure of tropical intraseasonal convection anomalies. J. Atmos. Sci. 47, 357–379.
Sanchez-Lavega, A., Lebonnois, S., Imamura, T., Read, P., Luz, D., 2017. The atmospheric dynamics of Venus. Space Sci. Rev. 212, 1541–1616.
Showman, A. P., Dowling, T., 2000. Nonlinear simulations of Jupiter's 5-micron hot spots. Science 289, 1737–1740.
Sobel, A., Maloney, E., 2012. An idealized semi-empirical framework for modeling Madden-Julian oscillation. J. Atmos. Sci. 69, 1691–1705.
Straub, K., Kiladis, G. N., 2002. Observations of a convectively coupled Kelvin wave in the Eastern pacific ITCZ. J. Atmos. Sci. 59, 30–52.
Tribbia, J., 1984. Modons in spherical geometry. Geophys. Astrophys. Fluid Dyn. 30, 131–168.
Verkley, W., 1984. The construction of barotropic modons on the sphere. J. Atmos. Sci. 41, 2492–2504.

Wang, D., Yano, J.-I., Lin, Y., 2019. Madden Julian oscillations seen in the upper-Troposphere vorticity field: interactions with Rossby wave trains. J. Atmos. Sci. 76, 1785–1807.

Wheeler, M., Kiladis, G., 1999. Convectively coupled equatorial waves: analysis of clouds and temperature in the wavenumberfrequency domain. J. Atmos. Sci. 56, 374–399.

Yanai, M., Chen, B., Tung, W.-W., 2000. The Madden – Julian Oscillation observed during the TOGA COARE IOP: Global View. J. Atmos. Sci. 57 (15), 2374–2396.

Yano, J.-I., Bonazzola, M., 2009. Scale analysis for large-scale tropical atmospheric dynamics. J. Atmos. Sci. 66, 159–172.

Yano, J.-I., Mulet, S., Bonazzola, M., 2009. Tropical large-scale circulations: asymptotically non-divergent? Tellus 61A, 417–427.

Yano, J.-I., Tribbia, J., 2017. Tropical atmospheric Madden–Julian Oscillation: a strongly nonlinear free solitary Rossby wave? J. Atmos. Sci. 74, 3473–3489.

Zeitlin, V., 2018. Geophysical Fluid Dynamics: Understanding (almost) Everything with Rotating Shallow Water Models. Oxford University Press.

Zhang, C., 2005. Madden-Julian oscillation. Rev. Geophys. 43, RG2003.

Zhang, C., Dong, M., 2004. Seasonality in the Madden – Julian oscillation. J. Climate 17 (16), 3169–3180.